ADVANCED ENERGY MATERIALS
www.advenergymat.de

High-Performance Fully Printable Perovskite Solar Cells via Blade-Coating Technique under the Ambient Condition

*Zhibin Yang, Chu-Chen Chueh, Fan Zuo, Jong H. Kim, Po-Wei Liang, and Alex K.-Y. Jen**

The exceptional photovoltaic properties demonstrated recently for organic–inorganic halide perovskites (such as $CH_3NH_3PbX_3$ (X = Cl, Br, or I)) have attracted great attention from researchers.[1–8] The promising features of these perovskites include broad and intense absorption spectra,[9] appropriate semiconducting properties,[10] long carrier diffusion length,[11,12] and facile solution processability, which enable improved power conversion efficiency (PCE) from 3.8%[13] to 20.1%[14] to be achieved within only a few years. The high efficiencies achieved in these solar cells are already on par with those made from multicrystalline silicon, CIGS, and CdTe.[14] In addition, all these highly efficient inorganic solar cells are usually fabricated with high vacuum and high temperature, which tend to increase production cost and impede their application on flexible substrates. These challenges can potentially be addressed by the emerging perovskite solar cells (PVSCs) because of their low-cost and low-temperature solution processability.

However, realizing fully printable PVSCs by large-area processing techniques is required before practical commercialization can be considered because most of the PVSCs studied so far are fabricated via the spin-coating method. Currently, several large-area device processing techniques have been developed for organic solar cells (OSCs), including spray-coating,[15] inkjet printing,[16] blade-coating,[17] screen printing,[18–22] and roll-to-roll printing.[23,24] All these methods have their own unique advantages. For instance, the spray-coating method can realize the deposition of extremely large area films with proper precursors effectively, the inkjet printing technique can achieve precise patterning and automatically repeating deposition with all kinds of setting programs, the screen printing can effectively achieve printing various size nanoparticle films to form the nanostructured scaffolds, and the roll-to-roll printing can allow effective in-line deposition for module fabrication. Although some of the above techniques have been employed for fabricating PVSCs,[24–30] the majority of the reports merely focus on printing the single perovskite layer, and the resulting devices often possess only small active areas for laboratory investigation. There are hardly any studies concerning fully printable PVSCs. Therefore, it is critical to demonstrate the feasibility of fabricating fully printable PVSC using large-area printing techniques, especially under ambient condition to pave the way for future mass production. Moreover, the quest of a throughout low-temperature printable technology is also highly desired in order to realize the flexible fully printable perovskite solar cells, which will represent an important milestone for the future practical applications.[31]

In order to fabricate large-area PVSCs, one of the critical challenges is to understand the influence of ambient environment on resultant perovskite thin-films since perovskite crystals are sensitive to humidity under ambient condition. It has been shown that perovskite crystals degrade gradually when they are in contact with ambient moisture for certain time.[31,32] Therefore, most of the high performance perovskite solar cells are prepared in glovebox to avoid contacting moisture. However, fabricating PVSCs under ambient condition is inevitable if we desire to transition from laboratory research into large-scale applications. Lately, there are several encouraging reports about allowing limited amount of moisture to facilitate the perovskite crystallization and improve the performance of resulting device.[33,34] However, there are no detailed underlying mechanisms explained on how moisture affects perovskite crystallization so far.

To alleviate these problems, we have investigated the feasibility of achieving fully printable PVSCs by the blade-coating technique under the ambient condition. The blade-coating fabrication has been widely used to fabricate OSCs and is proven to be a simple, environment-friendly, and low-cost method for the solution-processed photovoltaic. Compared to the screen printing, it not only can print nanoparticles, but also can print all kinds of solutions with any concentration. Moreover, the film morphology control of the blade-coating method is much better than the spray coating and roll-to-roll printing; high-quality photoactive layers with controllable thickness can be accomplished by using a precisely translational blade under the ambient condition with controlled relative humidity.

The PVSCs with a configuration of ITO/poly(3,4-ethylenedioxy-thiophene):poly(4-styrenesulfonate) (PEDOT:PSS)/$CH_3NH_3PbI_XCl_{3-X}$/[6,6]-phenyl-C_{61}- butyric acid methyl ester ($PC_{61}BM$)/Bis-C_{60}/Ag were fabricated to realize the fully printable process, as illustrated in **Figure 1**a. All constituent interlayers, except for the Ag top electrode, were prepared via blade-coating. The coating conditions were optimized to allow the preparation of high-quality interlayer films. Especially, the effect of humidity was carefully investigated and monitored to facilitate the crystallization of perovskite films under ambient condition. Finally, high PCE (10.44% ± 0.23%) device could be achieved after optimizing the blade-coating process and relative humidity in environment. Moreover, a high-performance flexible PVSC with a PCE of 7.14% ± 0.31% was demonstrated for the first time using this low-temperature (<150 °C) fully printable process.

Dr. Z. Yang, Dr. C.-C. Chueh, Dr. F. Zuo, Dr. J. H. Kim, P.-W. Liang, Prof. A. K.-Y. Jen
Department of Materials Science and Engineering
University of Washington
Seattle, WA 98195-2120, USA
E-mail: ajen@u.washington.edu

DOI: 10.1002/aenm.201500328

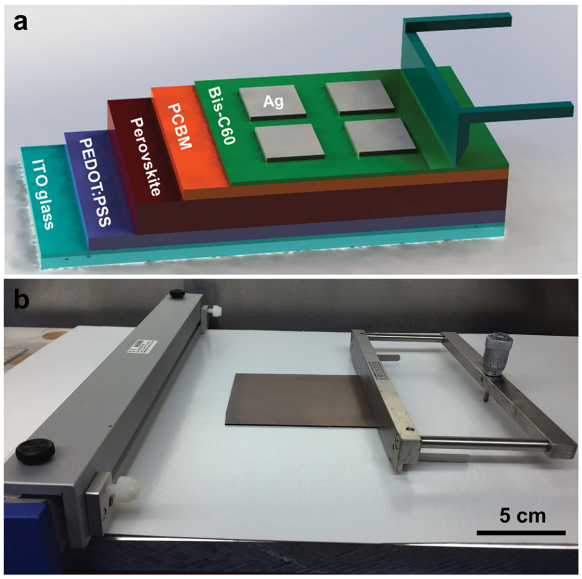

Figure 1. a) Schematic illustration of a fully printable perovskite solar cell. b) Blade-coating equipment with as-prepared 10 cm × 10 cm perovksite film.

To fabricate a fully printable PVSC under ambient condition, the targeted device layout is shown in Figure 1a and the corresponding energy level diagram is illustrated in Figure S1 (Supporting Information).[35,36] The blade coater used in this study is shown in Figure 1b. There are several challenges to overcome to realize blade-coated high PCE conventional p–i–n heterojunction PVSCs in ambient. First, a robust PEDOT:PSS layer needs to be printed on the ITO glass. However, the aqueous solution of PEDOT:PSS is very difficult to blade-coat smoothly due to its high surface tension. It needs to be diluted with isopropanol at a volume ratio of 1:3 for decreasing surface tension because isopropanol has lower surface energy (21.7 dyn cm^{-1}) compared to water (71.97 dyn cm^{-1}). Meanwhile, the surface energy of ITO can be reduced by UV ozone treatment to enrich the hydroxyl content on the surface. Consequently, the wetting between the diluted PEDOT:PSS solution and ITO glass is significantly improved. The ITO substrate temperature also needs to be maintained at 60 °C in order to achieve improved solvent volatilization for fast blade-coating of PEDOT:PSS to form homogenous film. Finally, an uniform and transparent PEDOT:PSS layer is prepared after annealing the blade-coated film at 150 °C for 10 min, as shown in Figure S2 (Supporting Information).

To prepare the perovskite photoactive layer, we adopted the one-step processing method to simplify the blade-coating process, in which the precursor solution was composed of CH_3NH_3I and $PbCl_2$ in anhydrous dimethyl formamide (DMF) at a molar ratio of 3:1. After blade-coating it onto PEDOT:PSS, thermal annealing was performed at 90 °C for 1 h and then another 1 h at 100 °C to complete the perovskite formation under ambient condition. It is important to mention that the blade-coating process can significantly retard the crystallization rate of derived perovskite films due to elongated drying time during the film formation. This is beneficial for forming homogeneous and highly crystalline perovskite films.[27] A

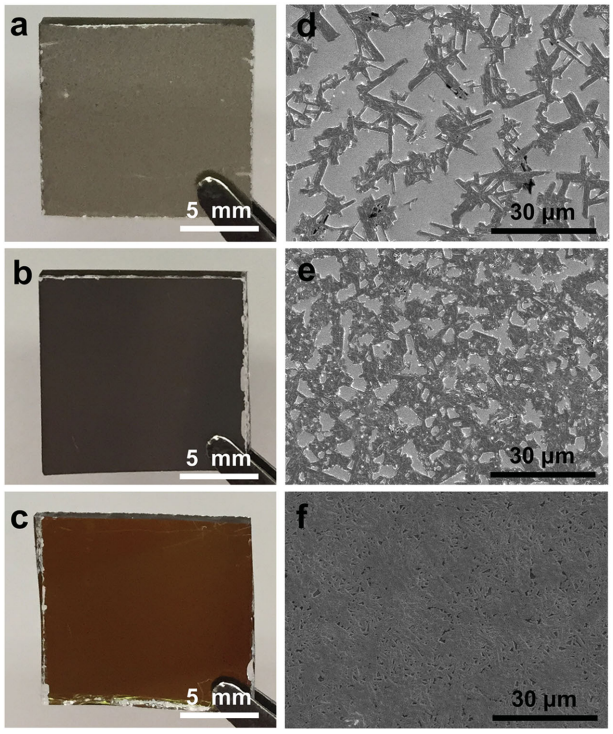

Figure 2. Photographs and SEM images of the perovskite films prepared by the blade-coating method under different humidity of a,d) 60%–70%, b,e) 40%–50%, and c,f) 15%–25%.

1,8-diiodooctane (DIO) additive was also added to the precursor solution to further modulate the morphology of perovskite films by improving the precursor solubility and prolonging the crystallization time as discussed earlier.[35,37] As shown in Figure 1b, a uniform 10 cm × 10 cm perovskite film can easily be prepared by this blade-coating process without wasting perovskite precursor compared to the spin-coating process. However, different relative humidity in ambient was found to play a significant role in affecting the quality and textures of the resulting perovskite films in the blade-coating process.

We speculate that humidity is the key factor that affects the perovskite film formation and resultant device performance. To clarify this, we have coated the perovskite films under ambient condition with varied relative humidity. As shown in **Figure 2**a–c, the color of the resultant perovskite films exhibits gray, black, and dark brown, respectively, when they were blade-coated under the varied humidity from 60–70%, 40–50% to 15–25%. This indicates that humidity in the atmosphere severely affects the nucleation and crystallization of perovskite during film evolution. The scanning electron microscopy (SEM) images (Figure 2d–f) show the distinct microstructures and morphologies of the corresponding perovskite films. As can clearly be seen, the coverage and homogeneity of the perovskite films are remarkably improved when the humidity in the environment is decreased from 60–70% to 15–25%. Figure S3 (Supporting Information) further compared the fine structure of the perovskite films prepared by the spin-coating method in nitrogen atmosphere and the blade-coating technique under ambient condition with humidity of 15%–25%. As can be seen, the morphology of the blade-coated film shows

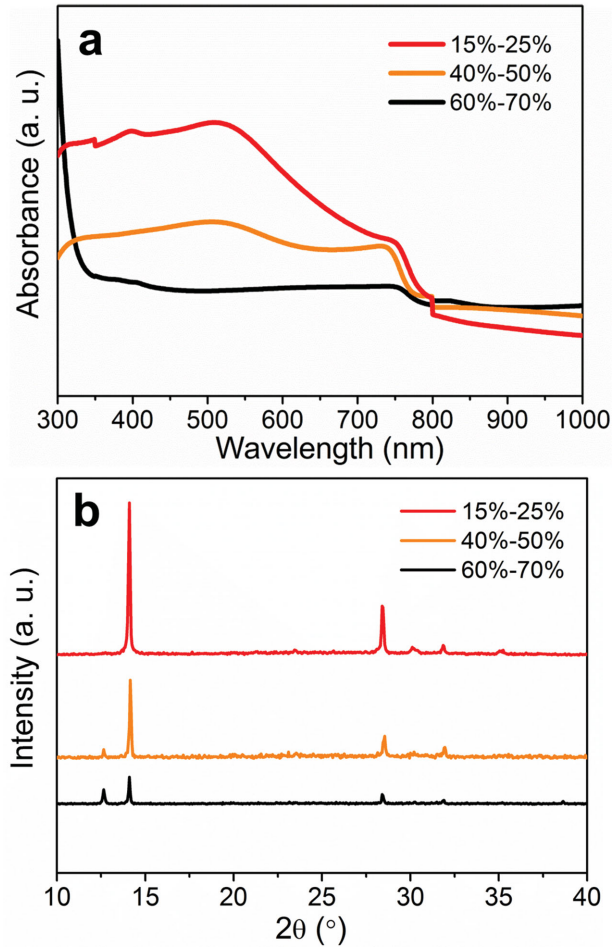

Figure 3. a) UV–vis absorption spectra and b) X-ray diffraction spectra of perovskite films prepared by blade coating method under different humidity of 60%–70%, 40%–50%, and 15%–25%.

a larger crystalline domain, while the spin-coated film shows better coverage.

The UV–vis absorption and X-ray diffraction (XRD) spectra shown in **Figure 3** also confirm this observed trend. As shown, the overall absorption of fabricated perovskite films gradually rises as the environmental humidity is decreased from 60–70% to 15–25% (Figure 3a), in which the increasing band-edge absorption around 780–790 nm also suggests the increased film crystallinity. The increased absorption can be attributed to the improved surface coverage and crystallinity in the perovskite films. The XRD patterns (Figure 3b and Figure S4, Supporting Information) of the blade-coated perovskite films show the tetragonal phase at room temperature.[38] The characteristic peaks at 14.2° and 28.5° corresponding to the (110) and (220) crystal planes become more dominant as the environmental humidity decreases, which indicates the improved crystallinity of the prepared perovskite films.

The participation of water in the crystallization process significantly affects the final crystal structure of perovskite. In the $CH_3NH_3PbI_XCl_{3-X}$-based perovskite, the $CH_3NH_3^+$ organic cation interacts with the PbI_3^- anion through hydrogen bonding between H–N/I^- and H–C/I^-. When the perovskite encounters a H_2O molecule, two stronger hydrogen bonds can be formed as O–H/I^- and O/N–H. According to the theoretical calculation performed by Dong et al.,[39] the stabilization energy of the O/N–H hydrogen bond is much larger than those of I^-/H–N and I^-/H–C in the $CH_3NH_3PbI_XCl_{3-X}$. In other words, the interaction between H_2O and $CH_3NH_3^+$ is much stronger than that between the $CH_3NH_3^+$ and PbI_3^-, which causes the degradation of perovskite. In the XRD spectra, a peak at 12.6°, which is the characteristic peak for PbI_2,[38] was observed to remarkably increase under the high humidity condition. It confirms that the participation of water molecules in perovskite tends to decompose its crystal structure.

Figure S5 (Supporting Information) shows PbI_2 that was formed from the perovskite degradation under a high humidity of 60%–70%. Nevertheless, we find that high-quality perovskite films can be obtained when it is annealed under low humidity of 15%–25% as shown in Figure 2c,f. We speculate that the incoming and evaporating H_2O molecules reach equilibrium to facilitate perovskite recrystallization during the annealing process. Therefore, water molecules do not affect the performance of perovskite films under low humidity.

After the deposition of perovskite, the fullerene-based interlayers were sequentially coated. The $PC_{61}BM$ and bis-C_{60} were dissolved in low boiling point chloroform and isopropanol, respectively, for the blade-coating process. Note that the function of $PC_{61}BM$ layer is to extract the electrons from the perovskite layer, while the bis-C_{60} interlayer serves both as an election extraction layer and a work function modifier simultaneously to enable better alignment of energy level between $PC_{61}BM$ and the electrode to facilitate electron collection and the use of stable Ag as a top electrode. Figures S6 and S7 (Supporting Information) show high-quality $PC_{61}BM$ and bis-C_{60} films prepared on the bare ITO substrate via the optimized blade-coating process.

It has been proven that surface coverage and crystallinity of perovskite film can significantly affect the resulting device performance because the defects in the crystals and the void in the films create severe charge recombination and shorting to deteriorate charge transport and collection. As expected, the PVSC fabricated under the humidity of 60%–70% exhibits a very poor photovoltaic performance with an open-circuit voltage (V_{OC}) of 0.37 V, a short-circuit current density (J_{SC}) of 2.98 mA cm^{-2}, a fill factor (FF) of 0.32, and a PCE (η) of 0.35% (**Figure 4**a). As the environment humidity drops to 40%–50%, the fabricated device shows an improved PCE of 3.63%. When the humidity was further decreased to 15%–25%, the PVSCs show a promising average PCE of 10.44% with a V_{OC} of 0.96 V, a J_{SC} of 16.73 mA cm^{-2}, and a *FF* of 0.65 (all the detailed parameters are summarized in **Table 1**).

As a comparison, a spin-coated PVSC with the identical device configuration was also fabricated, which exhibited an average PCE of 11.04% with a V_{OC} of 0.89 V, a J_{SC} of 16.85 mA cm^{-2}, and a *FF* of 0.73 (Figure S8, Supporting Information). The cross-section SEM image of the champion blade-coated device is shown in **Figure 5**, which illustrates a well-defined multilayered structure of PVSC with high uniformity of each constituent interlayer. The thicknesses of PEDOT:PSS, $CH_3NH_3PbI_XCl_{3-X}$, $PC_{61}BM$, bis-C_{60}, and Ag are 30, 350, 100, 30, and 120 nm, respectively. This result shows that the performance of a fully printable PVSC by blade-coating under con-

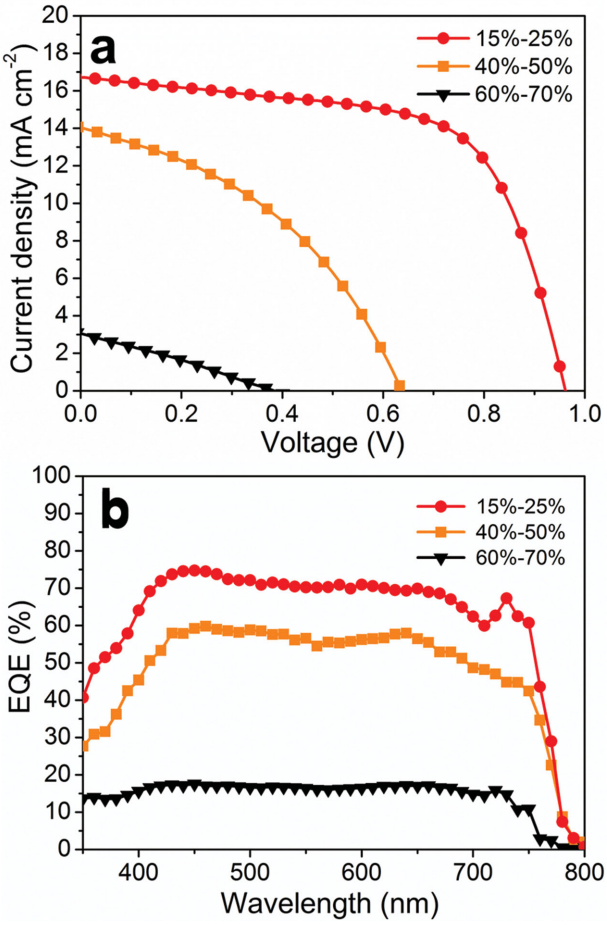

Figure 4. a) Typical *J–V* characteristics (measured under AM 1.5 illumination) and b) EQE spectra of perovskite solar cells prepared by the blade-coating method under different humidity of 60%–70%, 40%–50%, and 15%–25%.

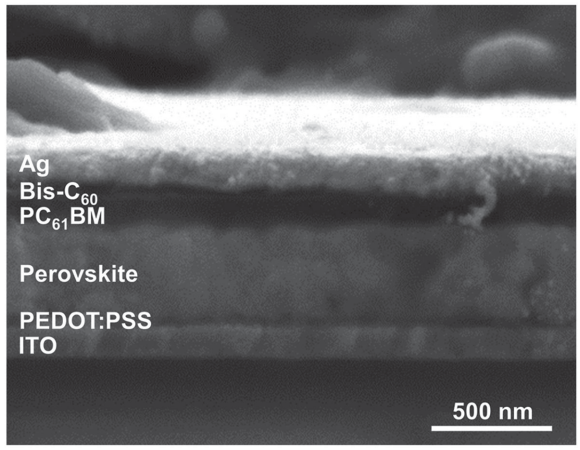

Figure 5. Cross sectional SEM image of a perovskite solar cell in a blade-coating method.

trolled ambient condition is comparable to those fabricated by spin-coating in the glove box. This signifies that it is feasible to use the blade-coating technique for large-scale PVSC applications in the future.

For the perovskite solar cells, anomalous hysteresis was often observed in their *J–V* cures.[40] Therefore, we have further examined the hysteresis phenomenon of the studied fully printable perovskite solar cells. As shown in Figure S9 (Supporting Information), the top-performing device exhibited insignificant hysteresis even measured under a very low scan rate of 0.01 V s^{-1}, suggesting the reliable performance of the fully printable perovskite solar cells via the blade-coating technique. Figure S10 (Supporting Information) shows the stability of the fully printable perovskite solar cells under different conditions. The device can maintain >90% of the original PCE after being stored for 10 d in inert atmosphere. However, the efficiency of the device decreased to ≈50% when it was stored under the ambient condition with 50% humidity. The degradation of the perovskite solar cells is inevitable when they are exposed to intensive moisture. Further encapsulation of the device is required for the future large-scale application.

In addition, the external quantum efficiency (EQE) spectra of the studied devices were also measured to evaluate the photon-to-electron conversion efficiency. As shown in Figure 4b, all three EQE curves present broad absorption characteristics ranging from 400 to 780 nm, and the values increase with the decease of humidity during device fabrication. For the top-performing PVSC printed under the humidity of 15%–25%, a high EQE value of 70% can be achieved.

Benefiting from the low-temperature blade-coating process of the targeted device, we have further fabricated a flexible PVSC on an ITO-coated poly(ethylene terephthalate) (PET) substrate, as illustrated in **Figure 6**a. This flexible device exhibits a V_{OC} of 0.87 V, a J_{SC} of 13.91 mA cm^{-2}, and a *FF* of 0.59, which results in a promising PCE of 7.14% (Figure 6b). Moreover, this flexible device can maintain 80% of the original PCE after being bended for 100 times with a bending radius of 1 cm (Figure S11, Supporting Information). The decreased PCE can be mainly

Table 1. Photovoltaic parameters of the perovskite solar cells fabricated under different humidity, which were measured under AM 1.5 illumination.

Humidity	V_{OC} [V]	J_{SC} [mA cm^{-2}]	*FF*	PCE [%]
60%–70%	0.37 ± 0.06	2.98 ± 0.91	0.32 ± 0.04	0.35 ± 0.16 (0.53%)
40%–50%	0.64 ± 0.03	14.04 ± 0.54	0.41 ± 0.03	3.63 ± 0.37 (4.07%)
15%–25%	0.96 ± 0.01	16.73 ± 0.43	0.65 ± 0.01	10.44 ± 0.23 (10.71%)
<0.1 ppm (spin-coating method)	0.89 ± 0.01	16.85 ± 0.23	0.73 ± 0.01	11.04 ± 0.19 (11.32%)
15%–25% (flexible solar cells)	0.87 ± 0.01	13.91 ± 0.41	0.59 ± 0.02	7.14 ± 0.31 (7.52%)

Average values with standard deviation (maximum values are indicated in parentheses).

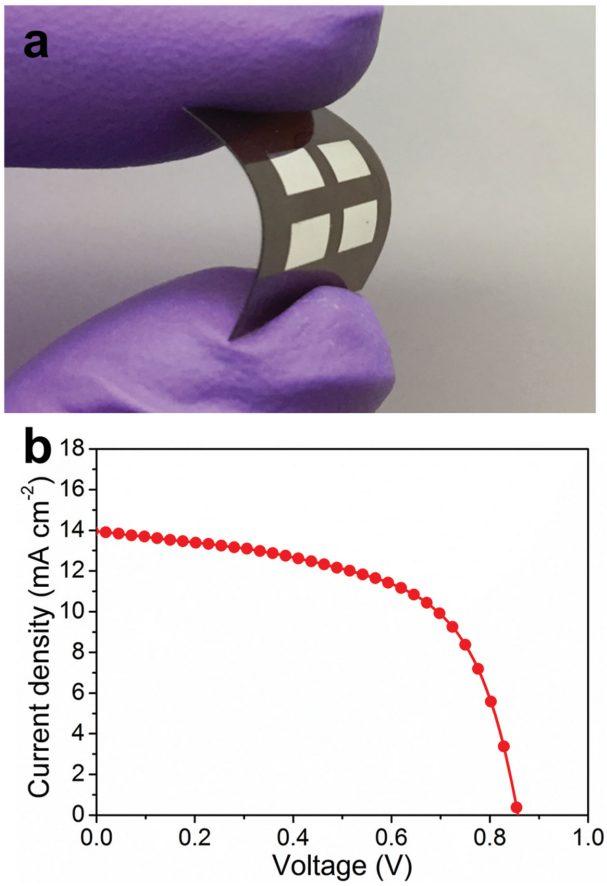

Figure 6. Photograph (a) and typical *J–V* characteristics (b) of a flexible perovskite solar cell prepared by blade coating method under humidity of 15%–25%.

attributed to the rigid and fragile property of the ITO substrates, which cracks easily during the bending test to result in degraded charge collection efficiency. To the best of our knowledge, this is the first demonstration of a fully printable flexible PVSC, which shows the potential of extending this process for roll-to-roll printing. Note that all the parameters obtained for the flexible PVSC are slightly inferior to those of the devices fabricated on a rigid ITO substrate. This is partially attributed to the relatively high sheet resistance of ITO/PET substrates (50 Ω sq^{-1}) than that of ITO glass (15 Ω sq^{-1}), causing higher series resistance. Moreover, the flexible substrate also created some handling difficulties during fabrication, which induced nonuniformity in the constituent layers. Therefore, further optimization is required to solve these problems.

In conclusion, a high-performance, fully printable PVSC has been demonstrated by using the blade-coating technique under ambient condition with controlled humidity. When the humidity is controlled at the level between 15% and 25%, the fabricated device exhibits a high PCE of 10.44%. More importantly, a flexible PVSC was demonstrated for the first time to afford a promising PCE of 7.14%. These results demonstrate the feasibility of fabricating large-area perovskite devices under ambient condition, which is very critical for large-scale production of high-performance PVSCs in the future.

Experimental Section

Materials: Lead chloride, DIO, and $PC_{61}BM$ were purchased from Sigma-Aldrich. Methyl ammonium iodide (CH_3NH_3I) was synthesized according to the reported method. Bis-C_{60} was synthesized as reported in our previous work.[41] The PEDOT:PSS solution was prepared by diluting PEDOT:PSS (Baytron PVP AI 4083) with isopropanol at a volume ratio of 1:3. The perovskite precursor solutions (20 wt%) were prepared by dissolving CH_3NH_3I and $PbCl_2$ into anhydrous dimethylformamide with a molar ratio of 3:1, followed by adding 1 wt% DIO to the resulting solution. Then, the perovskite precursor solution was stirred at 80 °C for 12 h. In addition, $PC_{61}BM$ solution (15 mg mL^{-1}) in chloroform and Bis-C_{60} surfactant solution (2 mg mL^{-1}) in isopropyl alcohol were separately prepared.

Device Fabrication: ITO glass (15 Ω sq^{-1}, 5 × 5 cm^2) and ITO/PET substrates (50 Ω sq^{-1}, 5 × 5 cm^2) were cleaned by sonication sequentially with detergent and deionized water, acetone, and isopropanol alcohol for 10 min, respectively. Then, the ITO glasses were further cleaned by a UV ozone cleaner for 5 min after drying with a nitrogen flow. Then, PEDOT:PSS solution (filtered with a 0.45 μm nylon filter, 50 μL) was blade-coated onto the substrates with a coating speed of 20 mm s^{-1} and blade–substrate gap of 50 μm at 60 °C, followed by annealing at 150 °C for 10 min in air (for the ITO/PET substrate, the PEDOT:PSS films were annealed at 100 °C for 15 min). After that, the perovskite precursor solution (filtered with a 0.45 μm PTFE filter, 80 μL) was blade-coated onto the substrate at 20 mm s^{-1} with the blade gap of 50 μm at room temperature. The resulting films on ITO glass were sequentially annealed at 90 °C for 1 h and at 100 °C for another hour. Then, the $PC_{61}BM$ solution (filtered with a 0.45 μm PTFE filter, 50 μL) was blade-coated onto the perovskite films with a coating speed of 20 mm s^{-1} and blade–substrate gap of 75 μm at 25 °C. Bis-C_{60} solution (filtered with a 0.45 μm PTFE filter, 50 μL) was blade-coated onto the $PC_{61}BM$ film with a coating speed of 20 mm s^{-1} and blade–substrate gap of 100 μm at 60 °C. All the blade-coating processes were performed under ambient condition with controlled humidity. Then, the resulting substrate was cut into pieces with size of 1.5 × 1.5 cm^2. At last, a 120 nm thick silver electrode was evaporated under high vacuum (<1 × 10^{-6} Torr) through a shadow mask. The fabrication details of spin-coated perovskite solar cells are the same as our previous report.[31] The effective areas of both blade-coated and spin-coated devices are 10 mm^2 defined by a mask. The relative humidity was controlled by a dehumidifier in a closed space.

Characterization: The blade-coating process was performed with a Coatmaster 510 (Erichsen). The structures of perovskite films were characterized by SEM (FEI Sirion SEM operated at 5 kV) and XRD (Bruker F8 Focus Powder XRD). The absorption spectra were measured by using a Varian Cary 5000 UV--vis--NIR. The *J–V* curves of the perovskite based solar cells were normally measured at a scan rate of 1 V s^{-1} with a forward scan by a Keithley 2400 Source Meter under illumination by an 450 Watt Oriel xenon lamp with an AM 1.5 G filter solar simulator simulated (100 mW cm^{-2}). The light intensity was precisely calibrated with a standard Si photodiode detector (equipped with a KG-5 filter) that can be traced back to the standard of the National Renewable Energy Laboratory. A mask was used to define the effective illuminated area. The EQE spectra were obtained from IPCE setup consisting of a Xenon lamp (Oriel, 450 W) as a light source, monochromator, a chopper with a frequency of 100 Hz, a lock-in amplifier (SR830, Stanford Research Corp), and Si-based diode (J115711-1-Si detector) for calibration.

Supporting Information

Supporting Information is available from the Wiley Online Library or from the author.

Acknowledgements

This work was supported by the Office of Naval Research (N00014-14-1-0246), the Department of Energy SunShot (DE-EE0006710), and

Washington Research Foundation Postdoctoral Research Program. A.K.-Y.J. thanks the Boeing-Johnson Foundation for financial support.

Received: February 13, 2015
Revised: March 30, 2015
Published online:

[1] S. Kazim, M. K. Nazeeruddin, M. Grätzel, S. Ahmad, *Angew. Chem. Int. Ed.* **2014**, *53*, 2812.
[2] M. A. Green, A. Ho-Baillie, H. J. Snaith, *Nat. Photonics* **2014**, *8*, 506.
[3] J. Burschka, N. Pellet, S.-J. Moon, R. Humphry-Baker, P. Gao, M. K. Nazeeruddin, M. Grätzel, *Nature* **2013**, *499*, 316.
[4] M. Liu, M. B. Johnston, H. J. Snaith, *Nature* **2013**, *501*, 395.
[5] Z. Xiao, C. Bi, Y. Shao, Q. Dong, Q. Wang, Y. Yuan, C. Wang, Y. Gao, J. Huang, *Energy Environ. Sci.* **2014**, *7*, 2619.
[6] J.-H. Im, I.-H. Jang, N. Pellet, M. Grätzel, N.-G. Park, *Nat. Nanotechnol.* **2014**, *9*, 927.
[7] D. Liu, T. L. Kelly, *Nat. Photonics* **2014**, *8*, 133.
[8] C. W. Chen, H. W. Kang, S. Y. Hsiao, P. F. Yang, K. M. Chiang, H. W. Lin, *Adv. Mater.* **2014**, *26*, 6647.
[9] H.-S. Kim, C.-R. Lee, J.-H. Im, K.-B. Lee, T. Moehl, A. Marchioro, S.-J. Moon, R. Humphry-Baker, J.-H. Yum, J. E. Moser, *Sci. Rep.* **2012**, *2*, 591.
[10] P.-W. Liang, C.-C. Chueh, X.-K. Xin, F. Zuo, S. T. Williams, C.-Y. Liao, A. K.-Y. Jen, *Adv. Energy Mater.* **2014**, *5*, 1400960.
[11] G. Xing, N. Mathews, S. Sun, S. S. Lim, Y. M. Lam, M. Grätzel, S. Mhaisalkar, T. C. Sum, *Science* **2013**, *342*, 344.
[12] S. D. Stranks, G. E. Eperon, G. Grancini, C. Menelaou, M. J. Alcocer, T. Leijtens, L. M. Herz, A. Petrozza, H. J. Snaith, *Science* **2013**, *342*, 341.
[13] A. Kojima, K. Teshima, Y. Shirai, T. Miyasaka, *J. Am. Chem. Soc.* **2009**, *131*, 6050.
[14] NREL Research cell efficiency records (accessed January 2015).
[15] D. Vak, S.-S. Kim, J. Jo, S.-H. Oh, S.-I. Na, J. Kim, D.-Y. Kim, *Appl. Phys. Lett.* **2007**, *91*, 081102.
[16] T. Aernouts, T. Aleksandrov, C. Girotto, J. Genoe, J. Poortmans, *Appl. Phys. Lett.* **2008**, *92*, 033306.
[17] Y.-H. Chang, S.-R. Tseng, C.-Y. Chen, H.-F. Meng, E.-C. Chen, S.-F. Horng, C.-S. Hsu, *Org. Electron.* **2009**, *10*, 741.
[18] A. Mei, X. Li, L. Liu, Z. Ku, T. Liu, Y. Rong, M. Xu, M. Hu, J. Chen, Y. Yang, M. Grätzel, H. Han, *Science* **2014**, *345*, 295.
[19] Z. Ku, Y. Rong, M. Xu, T. Liu, H. Han, *Sci. Rep.* **2013**, *3*.
[20] L. Zhang, T. Liu, L. Liu, M. Hu, Y. Yang, A. Mei, H. Han, *J. Mater. Chem. A* **2015**, DOI: 10.1039/C4TA04647A.
[21] Z. Yang, M. Liu, C. Zhang, W. W. Tjiu, T. Liu, H. Peng, *Angew. Chem. Int. Ed.* **2013**, *52*, 3996.
[22] Z. Yang, T. Chen, R. He, G. Guan, H. Li, L. Qiu, H. Peng, *Adv. Mater.* **2011**, *23*, 5436.
[23] F. C. Krebs, J. Fyenbo, M. Jørgensen, *J. Mater. Chem.* **2010**, *20*, 8994.
[24] K. Hwang, Y. S. Jung, Y. J. Heo, F. H. Scholes, S. E. Watkins, J. Subbiah, D. J. Jones, D. Y. Kim, D. Vak, *Adv. Mater.* **2015**, *27*, 1241.
[25] A. T. Barrows, A. J. Pearson, C. K. Kwak, A. D. Dunbar, A. R. Buckley, D. G. Lidzey, *Energy Environ. Sci.* **2014**, *7*, 2944.
[26] D. Vak, K. Hwang, A. Faulks, Y. S. Jung, N. Clark, D. Y. Kim, G. J. Wilson, S. E. Watkins, *Adv. Energy Mater.* **2014**, *5*, 1401539.
[27] S.-G. Li, K.-J. Jiang, M.-J. Su, X.-P. Cui, J.-H. Huang, Q.-Q. Zhang, X.-Q. Zhou, L.-M. Yang, Y.-L. Song, *J. Mater. Chem. A* **2015**, DOI: 10.1039/C4TA05675B.
[28] Z. Wei, H. Chen, K. Yan, S. Yang, *Angew. Chem. Int. Ed.* **2014**, *126*, 13455.
[29] A. Mei, X. Li, L. Liu, Z. Ku, T. Liu, Y. Rong, M. Xu, M. Hu, J. Chen, Y. Yang, *Science* **2014**, *345*, 295.
[30] J. H. Kim, S. T. Williams, N. Cho, C.-C. Chueh, A. K.-Y. Jen, *Adv. Energy Mater.* **2014**, *5*, 1401229.
[31] B. J. Kim, D. H. Kim, Y.-Y. Lee, H.-W. Shin, G. S. Han, J. S. Hong, K. Mahmood, T. K. Ahn, Y.-C. Joo, K. S. Hong, N.-G. Park, S. Lee, H. S. Jung, *Energy Environ. Sci.* **2015**, *8*, 916.
[32] S. N. Habisreutinger, T. Leijtens, G. E. Eperon, S. D. Stranks, R. J. Nicholas, H. J. Snaith, *Nano Lett.* **2014**, *14*, 5561.
[33] H. Zhou, Q. Chen, G. Li, S. Luo, T.-B. Song, H.-S. Duan, Z. Hong, J. You, Y. Liu, Y. Yang, *Science* **2014**, *345*, 542.
[34] K. K. Bass, R. E. McAnally, S. Zhou, P. I. Djurovich, M. E. Thompson, B. C. Melot, *Chem. Commun.* **2014**, *50*, 15819.
[35] P.-W. Liang, C.-Y. Liao, C.-C. Chueh, F. Zuo, S. T. Williams, X.-K. Xin, J. Lin, A. K. -Y. Jen, *Adv. Mater.* **2014**, *26*, 3748.
[36] F. Zuo, S. T. Williams, P.-W. Liang, C.-C. Chueh, C. Y. Liao, A. K.-Y. Jen, *Adv. Mater.* **2014**, *26*, 6454.
[37] C.-C. Chueh, C.-Y. Liao, F. Zuo, S. T. Williams, P.-W. Liang, A. K.-Y. Jen, *J. Mater. Chem. A* **2015**, DOI: 10.1039/C4TA05012F.
[38] C. C. Stoumpos, C. D. Malliakas, M. G. Kanatzidis, *Inorg. Chem.* **2013**, *52*, 9019.
[39] X. Dong, X. Fang, M. Lv, S. Zhang, J. Ding, N. Yuan, *J. Mater. Chem. A* **2015**, *3*, 5360.
[40] H. J. Snaith, A. Abate, J. M. Ball, G. E. Eperon, T. Leijtens, N. K. Noel, S. D. Stranks, J. T.-W. Wang, K. Wojciechowski, W. Zhang, *J. Phys. Chem. Lett.* **2014**, *5*, 1511.
[41] C.-Z. Li, C.-C. Chueh, H.-L. Yip, K. M. O'Malley, W.-C. Chen, A. K. -Y. Jen, *J. Mater. Chem.* **2012**, *22*, 8574.